Allogeneic Human Neural Stem Cells for Improved Therapeutic Delivery to Peritoneal Ovarian Cancer

*Jennifer Batalla-Covello[1,4‡], Wafa Abidi[2‡], Hoi Wa Ngai[1], Caitlyn Hyde[1], Diana Machado[1], Asma Abdul-Majid[1], Mohamed Hammad[1], Linda Flores[1], Greg Copeland[2], Thanh Dellinger[3], Ernest Han[3], Jacob Berlin[2], Karen S. Aboody[1], Rachael Mooney[1]**

[1]Department of Neurosciences, [2]Department of Molecular Medicine, [3]Division of Gynecologic Surgery, [4]Irell & Manella Graduate School of Biological Sciences Beckman Research Institute at City of Hope, 1500 East Duarte Road, Duarte, CA, 91010, United States

[‡]Jennifer Batalla-Covello and Wafa Abidi contributed equally to this manuscript.

***CORRESPONDING AUTHOR**: Rachael Mooney, Ph.D., City of Hope Familian Sciences 1014A, Department of Stem Cell and Developmental Biology, 1500 East Duarte Road, Duarte, California 91010, USA; Telephone: 626/256-4673 x84018; E-mail: rmooney@coh.org

ABSTRACT

Background: Immortalized, clonal HB1.F3.CD21 human neural stem/progenitor cells (NSCs), loaded with therapeutic cargo prior to intraperitoneal (IP) injection, have been shown to improve the delivery and efficacy of therapeutic agents in pre-clinical models of stage III ovarian cancer. In previous studies, the distribution and efficacy of the NSC-delivered cargo has been examined; however, the fate of the NSCs has not yet been explored. **Methods:** To monitor NSC tropism, we used an unconventional method of quantifying endocytosed gold nanorods to overcome the weaknesses of existing cell-tracking technologies. **Results:** Here, we report efficient tumor tropism of HB1.F3.CD21 NSCs, showing that they primarily distribute to the tumor stroma surrounding individual tumor foci within 3 hours after injection, reaching up to 95% of IP metastases without localizing to healthy tissue. Furthermore, we demonstrate that these NSCs are non-tumorigenic and non-immunogenic within the peritoneal setting. **Conclusions:** Their efficient tropism, combined with their promising clinical safety features and potential for cost-effective scale-up, positions this NSC line as a practical, off-the-shelf platform to improve the delivery of a myriad of peritoneal cancer therapeutics.

KEYWORDS: Neural Stem Cells, Ovarian Cancer, Peritoneal Metastases, Tumor Tropism, Cell Therapy, Drug Delivery

BACKGROUND

Ovarian cancer is a deadly disease that afflicts approximately 22,000 women in the United States per year [1]. For patients with stage III ovarian cancer, in which tumors have metastasized to the abdominal cavity, the five-year survival rate is only 34% [1]. Intraperitoneal (IP) chemotherapy confers a significant survival advantage in these patients, but its widespread use has been limited by its toxic side effects, which often prevent treatment completion. A targeted delivery system to concentrate therapeutics specifically at ovarian tumor sites could substantially enhance treatment efficacy and reduce undesirable side effects, improving quality of life.

Tumor-tropic cell carriers, which have a propensity to migrate to tumor sites, have shown promise as a tumor-targeted delivery system. For example, we and others have demonstrated that cell carriers afford advantages over free nanoparticle (NP) delivery in the IP cavity. Specifically, mesenchymal stem cells (MSCs), neural stem/progenitor cells (NSCs), T-cells, and macrophages can dramatically increase the efficiency and number of therapeutic NPs that localize to tumors *in vitro* and *in vivo* [2-6]. Cell-mediated tumor tropism is not passive, but rather an active, discriminating process mediated by a myriad of tumor-localized signals [7]. Because cell carriers are approximately 10 μm in diameter, they mainly deposit on the peritoneal surface rather than pass through it [8, 9]. Furthermore, cell carriers injected into the IP cavity can increase the retention of small (~100-nm) NPs from mere hours to several days [10].

Autologous MSCs, which have been the predominant cell type investigated for peritoneal therapeutic delivery [11, 12], can be isolated from a patient's bone marrow or adipose tissues, expanded and modified *ex vivo*, and re-administered. However, there are major drawbacks to the use of MSCs, including that they are composed of heterogeneous cell populations, have poorly reproducible *ex vivo* loading capacities, and lose their tumor-homing properties after 5–6 passages [12]. Moreover, the amount and quality of MSCs that can be isolated depend critically on patient age and health status, and it can take two weeks after isolation to generate a sufficient number of cells for treatment [12]. In addition, it was recently reported that 20% of expanded MSCs had abnormal karyotypes [12], which is of deep concern as the confirmed non-tumorigenicity of any clinical

stem cell therapy is of paramount importance. Consequently, although autologous MSCs may be feasible therapeutic delivery vehicles for smaller phase I trials, they represent an inefficient and poorly reproducible approach that will be difficult to pass through regulatory hurdles and meet the scale-up requirements necessary for phase II and III trials [12]. Therefore, developing a more clinically viable strategy to deliver therapeutic cargo selectively to tumor sites is critical.

In our previous work [13, 14], we investigated the use of an established tumor-tropic human clonal NSC line, HB1.F3.CD21, for targeted IP therapy in orthotopic mouse models of high-grade serous ovarian cancer, the most common histotype of stage III peritoneal disease. These NSCs are chromosomally and functionally stable over time and passage, HLA class II-negative, and their clinical safety, tumor tropism, and tumor-localized chemotherapy production in recurrent glioma patients has been demonstrated [15]. Importantly, this NSC line has established standard operating procedures for scaled-up production that are more efficient, reproducible, and economical than those used for autologous cells. Thus, the line can be expanded, modified, and banked as an "off-the-shelf" product, readily available for trials at multiple sites [16]. Although we previously demonstrated that the IP administration of these NSCs improves the delivery and therapeutic efficacy of drug-loaded NPs [13, 14] and oncolytic viruses [17] in ovarian metastases, additional studies are required to determine the efficiency of each administration, degree of tumor coverage, penetration of the tumor stroma, and potential unintended tumorigenic/immunogenic effects of these NSCs.

In the present study, we conduct comprehensive pharmacokinetic and biodistribution assessments to probe the efficiency, peritoneal distribution, tumorigenicity, and immunogenicity of this NSC-based therapeutic delivery platform. We investigate NSC tumor tropism in both immunodeficient and immunocompetent orthotopic mouse models of IP ovarian metastases. Using these models, we confirm our previous observation that NSCs localize only to tumor nodules and not to normal tissues [13, 17]. We also demonstrate that HB1.F3.CD21 NSCs target ovarian metastases with remarkable efficiency and selectivity, positioning this cell line as an excellent delivery platform to improve the therapeutic index of IP anticancer treatments.

METHODS:

Cell Culture: The *v*-myc immortalized, clonal human HB1.F3.CD21 NSC line (approved by the Food and Drug Administration for human glioma clinical trials via local injection, Identifier: NCT01172964), was obtained from Dr. Seung Kim (University of British Columbia, Canada). The NSCs were further modified to produce NSC.eGFP.ffluc cells expressing green fluorescent protein (eGFP) and firefly luciferase (ffluc), as previously described [18]. The ID8 murine ovarian cancer line was obtained from Dr. Katherine Roby (University of Kansas). These cells were further modified using a PJ01668-eGFP-ffluc-epHIV7 lentiviral vector (159e6 TU/ML; VF0716) generously provided by Dr. Christine Brown (City of Hope) to produce ID8.eGFP.ffluc cells. Reporter gene expression and tumorigenicity were confirmed for the ID8.eGFP.ffluc line prior to study initiation (Supplementary Figure 1). eGFP and ffluc-expressing OVCAR8 human ovarian cancer cells (OVCAR8.eGFP.ffluc) were generously provided by Dr. Carlotta Glackin (City of Hope). The NSC and ID8 cell lines were cultured in DMEM (Invitrogen) and the OVCAR8 cell line was cultured in RPMI basal media; all media was supplemented with 10% fetal bovine serum (Gemini Bio), 1% L-glutamine (Invitrogen), and 1% penicillin-streptomycin (Invitrogen). All cells were maintained at 37°C in a humidified incubator (Thermo Electron Corporation) containing 6% CO_2 and passaged using a 0.25% trypsin and EDTA solution (Invitrogen) when they reached 80% confluency, and media was changed every 2–3 days.

In Vivo NSC Administration and Tracking in Ovarian Cancer Models: Mice were maintained under specific pathogen-free conditions in the City of Hope Animal Resource Center, an AAALAC-accredited facility. All procedures were reviewed and approved by the City of Hope Animal Care Committee. For our immunodeficient model, 6–8-week-old female nude mice (The Jackson Laboratory) were inoculated with 2×10^6 OVCAR8.eGFP.ffluc cells via IP injection. For our immunocompetent model, 7–8 week old female C57Bl/6 mice (B6, National Cancer Institute [NCI]) were inoculated with 5×10^6 ID8.eGFP.ffluc cells via IP injection. After tumor development (3 weeks for OVCAR8, and 6 weeks for ID8), mice received NSCs

(10,000–1 × 10^7 total) labeled with lipophilic tracers (DiR; Thermo Fisher Scientific), 811-nm MUTAB-conjugated gold nanorods (AuNRs; Nanopartz), or cisplatin-containing mesoporous silica NPs (Cis.NPs, fabricated at City of Hope, as previously described [13]). At select time points after administration of NSCs, mice underwent live-animal imaging (described below), then peritoneal lavage fluid was collected, as previously described [19], and tumors were harvested from major organs (liver, kidney, stomach, intestines, and mesentery) and processed for inductively coupled plasma mass spectrometry (ICP-MS) quantification or fluorescence imaging, as described below.

Live-Animal Imaging: Tumor burden and NSC localization were evaluated via bioluminescence imaging. To determine if AuNRs affect NSC viability or tropism *in vivo*, OVCAR8.eGFP.ffluc tumor cells were used to inoculate nude mice and DiR-labeled NSCs with or without AuNRs were injected IP. To track NSC clearance in another experimental subset of mice, unlabeled tumor cells were used to inoculate nude mice, and DiR-labeled NSC.eGFP.ffluc cells were inject IP. Prior to imaging, mice were anesthetized by isoflurane (1.5 L/oxygen, 4% isoflurane) in an induction chamber and injected IP with D-luciferin substrate suspended in PBS at 4.29 mg/mouse. Mice were maintained under anesthesia in chamber, and NSCs were imaged 7 min after luciferin injection using a SPECTRAL Ami X charge-coupled device camera coupled to Ami X image acquisition and analysis software. Light emission was measured over an integration time of 30 s.

ICP-MS Quantification of AuNRs: Concentrations of gold (AuNRs) in tumors and peritoneal lavage fluid were determined using an Agilent 8800 inductively coupled plasma triple quadrupole mass spectrometer. Briefly, each sample was digested with 70% HNO_3 at 80°C for 16 h. Samples were diluted with 2% HNO_3 prior to injection into the mass spectrometer, and the detected signals were determined based on standard curves made using serial dilutions of gold (100 ppm) standard solutions (Spex Certiprep) in 1% HCl and 2% HNO_3. To determine the percentage of AuNRs that localized to tumors vs. the lavage fluid, their concentrations were normalized to the concentrations detected in the original cell suspension that was injected into each mouse.

Fluorescence Imaging: Tumors were frozen in Tissue Tek OCT (Sakura Finetek USA) and sectioned

147 on a Leica CM1510 S cryostat (Leica Biosystems). Sections (10 μm) were collected on positively charged slides
148 (Thermo Fisher Scientific), immunostained for active caspase-3/7 (AB3626; Chemicon), counterstained with
149 DAPI (1 μg/mL; Sigma), and imaged using a Zeiss Axio Observer Z1 fluorescence microscope (Zeiss
150 Microscopy). For 3D histological reconstruction to visualize NSC penetration, a subset of tumors was sectioned
151 into 10μm thick slices, imaged in their entirety at 200 μm intervals, and virtually reconstructed using
152 Reconstruct software [20].

153 ***Mixed Lymphocyte Reaction:*** To assess the immunogenicity of the NSCs *in vitro*, peripheral blood
154 mononuclear cells (PBMCs) were incubated with NSCs and their degranulation measured, as previously
155 described [21]. Briefly, PBMCs were isolated from seven healthy volunteers, using standard Ficoll density
156 gradient centrifugation, and cryopreserved. Thawed aliquots of PBMCs were co-cultured with NSCs (1:1 final
157 ratio), and FITC-conjugated antibodies against CD107a and CD107b (BD Pharmingen) were added to the
158 cultures, followed by a monensin-containing protein transport inhibitor (GolgiStop; BD Biosciences). Cells
159 were then stained with antibodies against CD3, CD4, CD56, CD16, CD14, and CD19 (BD Pharmingen) and
160 analyzed using a Gallios flow cytometer (Beckman Coulter). Monocytes and B cells that expressed CD14 and
161 CD19 were excluded. PBMCs stimulated with phorbol myristate acetate (PMA; 50 ng/ml) and
162 phytohemagglutinin (PHA; 1 μg/ml) served as positive controls.

163 ***Flow Cytometric Analysis of PD-L1 and CD47 Expression:*** Trypsinized NSCs were stained with
164 PE/Dazzle594-conjugated antibodies against human PD-L1 (clone 29E2A3) and CD47 (clone CC2C6) and their
165 respective isotype controls (BioLegend). All flow samples were acquired using a Guava EasyCyte flow
166 cytometer (Millipore). Histograms were generated using FlowJo (Tree Star).

167 ***Tumorigenicity:*** To determine if IP injections of NSCs altered tumor progression *in vivo*, nude mice
168 were inoculated IP with OVCAR8.eGFP.ffluc cells. After allowing tumors to progress unaltered for one or three
169 weeks (early and late tumor stages, respectively), mice received IP injections of 2×10^7 NSCs twice a week for
170 three weeks. After the last week of treatment, mice were euthanized and tumors harvested, pooled, and weighed

in pre-tared tubes.

Statistical Analysis: Data are presented as mean ± SEM, and statistical significance (p <0.05) was determined using two-tailed Student's t-tests.

RESULTS

AuNR-based Tracking of NSC Tumor Tropism Within the Peritoneal Cavity: In mouse models, tumor cells inoculated into the peritoneal cavity are carried by the physiological movement of the peritoneal fluid to seed the greater omentum, followed by the serosal surfaces of the liver, kidney, intestines, diaphragm, and peritoneum. The tumors that are formed consist of small (0.5–5-mm) nodules scattered over the peritoneal surface. Thus, it was necessary to identify a tracking method that is sensitive enough to quantify the presence of NSCs at individual nodules. In preliminary studies, we found that the signal afforded by membrane dyes and fluorescent gene markers was suboptimal for the sensitive quantification of NSCs localized to IP tumors. Instead, we labeled NSCs with internalized AuNRs **(Fig. 1A)**, which provide an NSC-specific signal that can be assessed quantitatively with high sensitivity using ICP-MS.

We previously showed that AuNRs do not impair NSC viability or tropism *in vitro* [22, 23]. Here, we utilized live-animal imaging to demonstrate that DiR-stained NSCs labeled with AuNRs are able to migrate towards tumors within the peritoneal setting *in vivo* **(Fig. 1B)**. We then determined the limits of AuNR detection and verified the dose-responsiveness of our AuNR-based NSC quantification method. The minimum number of NSC.AuNRs required to produce measurable AuNR levels in harvested tumors (pooled) was about 100,000 **(Fig. 1C)**, and detection was dose-responsive up to an injected dose of 1×10^7 NSCs, which is the maximum practical dose based on scale-up considerations for human trials **(Fig. 1C)**.

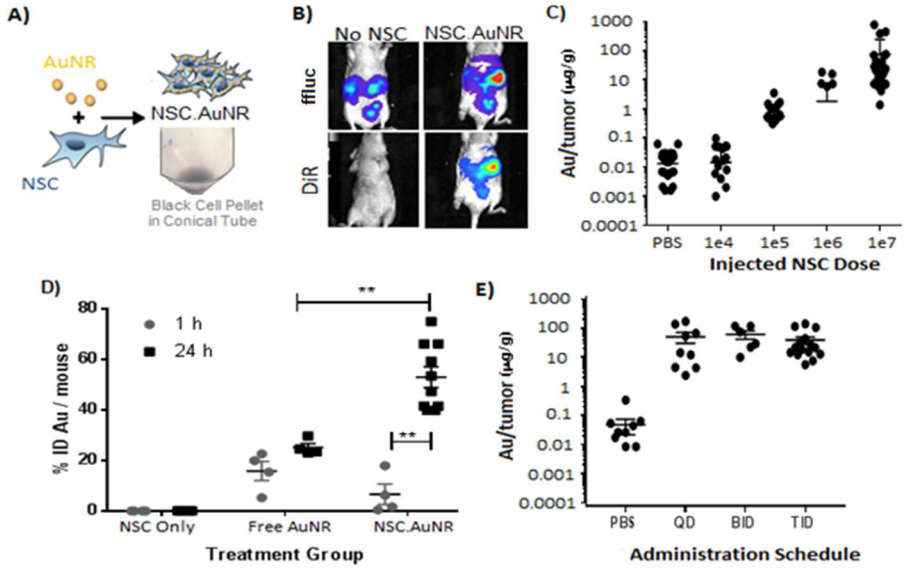

Figure 1: AuNR-based monitoring of HB1.F3.CD21 NSC tropism to peritoneal metastases. (A) Schematic showing AuNR-loaded NSCs (NSC.AuNRs), which are visibly black at the bottom of the conical tube shown in the photograph. **(B)** Fluorescent and bioluminescent images confirming that DiR-labeled NSC.AuNRs (bottom panel) co-localize with ffluc-expressing tumors (top panel). Nude mice were inoculated with 2×10^6 OVCAR8.eGFP.ffluc tumor cells, and NSC.AuNRs, dual-labeled with DiR to track their distribution, were injected three weeks later. Images were acquired one hour after IP NSC.AuNR injection. **(C–E)** ICP-MS quantification of AuNR levels within IP metastases. **(C)** ICP-MS quantification of tumor-localized NSC.AuNRs in a titration experiment demonstrating the limits and linear dose-response relationship of NSC.AuNR detection within the IP cavity. **(D)** AuNR quantification as a percentage of signal in the injected dose [%ID] of either free AuNRs or NSC.AuNRs at 1 and 24 h after injection. $^{**}p < 0.01$. **(E)** ICP-MS quantification of 1×10^7 NSC.AuNRs total, administered over 24 h via one (QID), two (BID), or three (BID) injections.

To determine the efficiency with which NSC.AuNRs migrate to IP tumors, we quantified the AuNR content within suspensions of 1×10^7 NSCs, which were then injected into the peritoneal cavities of nude mice bearing OVCAR8 tumors. Tumors were harvested from mice at 1 and 24 h after NSC injection to assess their AuNR content. ICP-MS analysis revealed that 60% ± 20% of the injected dose was localized to the tumors by 24 h **(Fig. 1D).** To confirm that the tumor-localized AuNR signal could be attributed to NSCs, we also evaluated control mice injected with a matching dose of free AuNRs and observed a signal 52 ± 13% lower than that of the NSC.AuNRs at 24 h.

We next tested if NSC localization to tumor sites could be enhanced by splitting the dose of 1×10^7 NSC.AuNRs into two or three injections administered over a 24 h period **(Fig. 1E)**. We found no significant

differences in the quantity of NSC.AuNRs localized to the tumor when they were administered as a single bolus dose rather than in multiple injections.

Kinetics of NSC Tropism and Cargo Delivery: The migration of NSCs from the peritoneal cavity to the tumors could be observed macroscopically, because the AuNRs are visibly black. This resulted in localized NSCs altering the tumor appearance from white to grayish within 24 hours **(Fig. 2A)**. Conversely, the pellet of cells harvested from the lavage fluid was black soon after IP administration of NSC.AuNRs but white within 24 hours **(Fig. 2A)**. To further evaluate NSC tropism kinetics, we quantified gold levels within tumors and peritoneal lavage fluid collected at several time points after IP administration of NSC.AuNRs in OVCAR8 tumor-bearing nude mice. ICP-MS analysis demonstrated that 60 ± 20% of the NSC dose localized to tumors within 2–3 h after IP administration **(Fig. 2B)**. At all tested time points (1–72 h), 70–80% of the injected NSCs were accounted for in either the lavage fluid or the tumors.

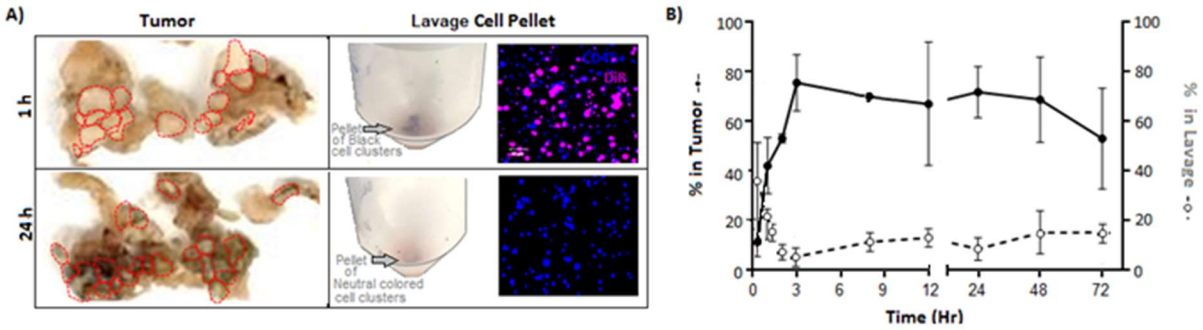

Figure 2: NSC tropism kinetics. (A) Photographs of ovarian tumor nodules (left panel, outlined in red) and centrifuged lavage cell pellets (center panel) after IP administration of 1×10^7 DiR-labeled NSC.AuNRs, demonstrating the localization of black NSCs in the lavage fluid at 1 h and in tumors at 24 h. The lavage cell pellets were also imaged with fluorescence microscopy (right panel) to visualize the number of DiR-labeled NSC.AuNRs (magenta) at each time point. Anti-CD45 antibodies were used to visualize macrophages (blue). **(B)** ICP-MS quantification of NSC-delivered AuNRs within ovarian metastases (solid lines) and peritoneal lavage fluid (dashed lines) over a 72-h period following IP NSC administration into tumor-bearing nude mice.

NSC Tumor Coverage and Biodistribution: To assess the extent of NSC tumor coverage, we isolated individual IP tumor nodules and used ICP-MS to determine the number of NSCs contained therein. After IP administration of 1×10^7 NSC.AuNRs to immunodeficient (nude) or immunocompetent (B6) mice bearing

peritoneal ovarian metastases (OVCAR8 and ID8, respectively), more than 95% of tumor metastases were found to contain at least 10 NSCs, with each tumor containing a median of 425 NSCs **(Fig. 3A)**. We also evaluated the distribution of NSC.AuNRs across tumors associated with specific organs. AuNR levels were particularly high in the omentum **(Fig. 3B)**, the primary site of ovarian cancer metastases in patients [24], which accounted for approximately 40% of the collected tumor tissue by mass. To evaluate the distribution of NSCs within individual tumor nodules, we performed serial cryosectioning, fluorescence imaging, and 3D tumor reconstruction. The NSCs were generally distributed at the peritumoral stroma, with some penetration into the tumor parenchyma if there was also stromal infiltration **(Fig. 3C–D).** No obvious off-target distribution was observed in any cryosectioned tissue samples. NSC.AuNR distribution to the tumor-associated stroma was observable macroscopically as a grayish colored tissue connecting individual tumor metastasis **(Fig. 3E).**

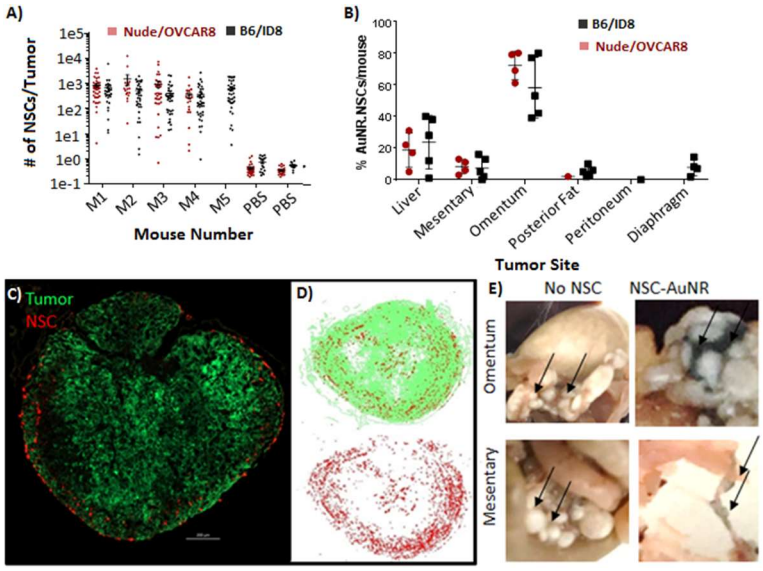

Figure 3: NSC biodistribution within the IP cavity. (A, B) ICP-MS quantification of NSC tumor tropism efficiency within immunodeficient (nude/OVCAR8) and immunocompetent (B6/ID8) mice. **(A)** The absolute number of NSCs localized to individual macroscopic tumors was determined based off a measurement of 5pg AuNR/NSC. **(B)** Localization of NSC.AuNRs in tumors associated with specific organs, expressed as a percentage of the total number of tumor-associated NSCs. Each data point is the summed percentage present in each mouse analyzed in 3A. **(C–E)** Distribution of IP-administered NSCs in the tumor parenchyma and peritumoral stroma. **(C)** Representative fluorescence microscopy image of an ovarian tumor nodule (green) and surrounding NSCs (red). **(D)** Flattened (top-down) 3D rendering of the distribution of NSCs throughout a single tumor nodule in Fig. 3C. **(E)** Photographs representative of tumors found on all organs demonstrating the presence of visibly black tumor-associated NSC.AuNRs localized to peritumoral stroma, 24 h after injection into OVCAR8 tumor-bearing nude mice.

NSC Clearance Kinetics: Once localized to tumors, the NSCs remained present for at least 3–11 days, according to steady NSC-associated AuNR and DiR signals **(Fig. 2B 4A)**. However, these NSCs appeared to die quickly, as evidenced by a steep decline in ffluc expression **(Fig. 4A)** and increased caspase-3/7 (apoptotic) activity in NSCs on day 11 **(Fig. 4B)**.

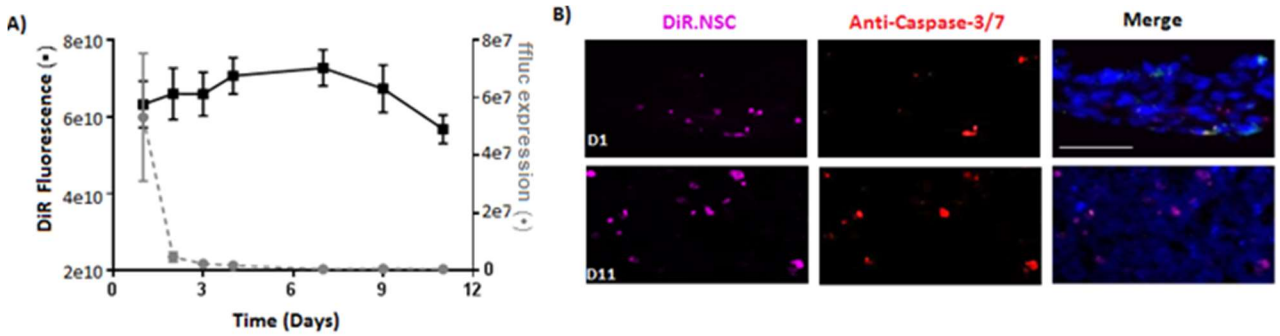

Figure 4: NSC clearance kinetics. (A) Retention and viability of DiR-labeled NSC.eGFP.ffluc cells over a two-week period following IP injection into tumor-bearing nude mice (solid line, DiR fluorescence; dotted line, ffluc expression). **(B)** Fluorescent images of sectioned tumors obtained either 1 day (D1) or 11 days (D11) after IP injection of NSCs (magenta). Anti-caspase-3/7 antibodies were used to visualize apoptosis (red); cells were counterstained with DAPI (blue). Scale bar = 50 μM and applies to all images.

NSC Immunogenicity and Tumorigenicity: HB1.F3.CD21 NSCs are generally considered to have negligible immunogenicity. They inherently express low levels of MHC class I antigens and undetectable levels of MHC class II antigens. We observed negligible immunological recognition of parental NSCs by PBMCs *in vitro* **(Fig. 5A)**. The NSCs also had low expression of PD-L1 and CD47 (Fig. 5B), presumably reducing their visibility to the innate and adaptive immune systems, respectively. In addition, we demonstrated that bi-weekly IP administrations of 2×10^7 NSCs (greater than the maximum clinical dose) did not promote ovarian tumor growth in immunodeficient (nude) mice bearing early- or late-stage OVCAR8 tumors (**Fig. 5C**).

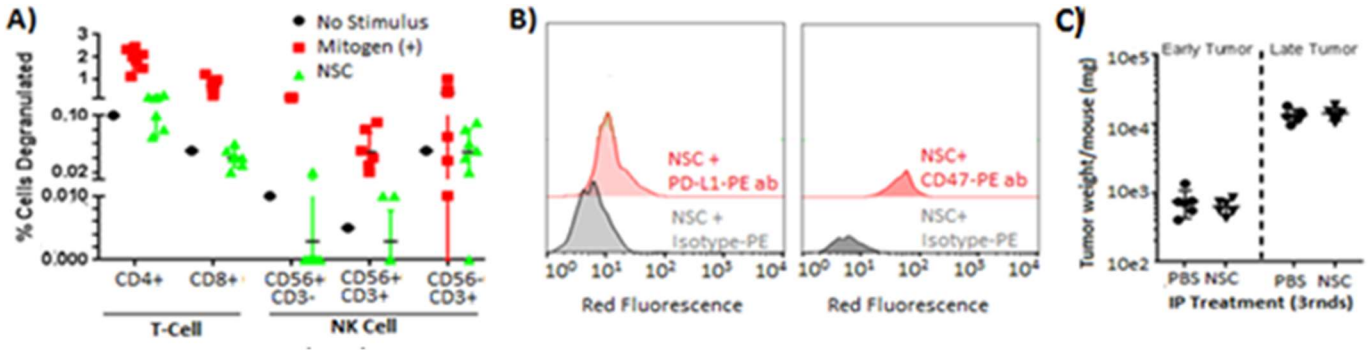

Figure 5: Immunogenicity of NSCs. (A) Fractions of CD107a/b-positive cytotoxic T-lymphocytes (CD3+, CD8+), T-helper lymphocytes (CD3+, CD4+), and natural killer cells (CD56+, CD3-) in response to NSC exposure. The City of Hope Clinical Immunobiology Correlative Studies Laboratory obtained whole blood from normal human donors (n = 7), isolated PBMCs via Ficoll density gradient centrifugation, then co-cultured them with NSCs in the presence of antibodies against CD107a/b. Positive control PBMCs were exposed to PMA and PHA. After a 5-h incubation period, flow cytometry was performed, with compensation for non-viable cells and isotype controls. **(B)** Flow cytometric quantification of PD-L1- and CD47-positive NSCs. **(C)** Pooled weights of macroscopic OVCAR8 tumors, as well as their associated stroma, in nude mice after three weekly rounds of 2×10^7 NSCs given 2x/week (for a combined total of 12×10^7 NSCs). Treatment started after one week or three weeks after tumor cell inoculation to evaluate early- and late-stage tumors, respectively.

DISCUSSION

Collectively, our results demonstrate the remarkable extent to which HB1.F3.CD21 NSCs rapidly and selectively home to an overwhelming majority of peritoneal metastases. Here, we discuss our major findings in the context of current literature.

NSCs Localize Efficiently to Peritoneal Metastases: Although IP-administered NSCs have the potential to migrate anywhere on the vast peritoneal surface area (1.7 m^2), our ICP-MS based quantification of NSC-associated AuNRs unexpectedly showed that an impressive 70–80% of NSCs localized to tumors, reaching up to 95% within 3 h after injection (**Fig.2B,3A**). One possible explanation for this tumor-specific localization is that the healthy mesothelium is protected by a layer of anti-adhesive proteoglycans [23], whereas tumor disruptions expose the underlying basement membrane, revealing extracellular matrix substrates (e.g., collagen I/IV, fibronectin, hyaluronan, and laminin [26]) that can be bound by CD44 [25] and $\alpha_5\beta_1$ integrins [26] expressed by the HB1.F3.CD.21 NSCs. Because this study focused only on intra-abdominal tumors and peritoneal lavage fluid, we were unable to account for the distribution of approximately 20% of injected NSCs.

303 A minority of these NSCs may have been cleared from the abdomen through either the general circulation or
304 lymphatic systems.

305 We used the unconventional method of quantifying endocytosed AuNRs to monitor NSC tropism in
306 order to overcome the weaknesses of existing cell-tracking technologies. Although the NSCs are engineered to
307 express both eGFP and ffluc, given the resolution limits of live-animal imaging, these markers do not permit
308 sensitive, quantitative NSC detection. Furthermore, tumor and stromal DNA/cell counts overwhelm NSC-
309 specific signals, so the number of NSCs present in tumor tissues is not reliably discernable using PCR or FACS.
310 In addition, membrane dyes cannot be used without a complementary approach due to the possibility of dye
311 transfer from injected cells to host cells [27]. In contrast, inorganic NP trackers provide a better balance of
312 sensitivity, dynamic range, and stability for assessing the distribution of IP-administered NSCs. Importantly,
313 this method also enables the macroscopic observation of NSC migration, as well as the ability to assess NSC
314 cargo delivery (**Fig. 1A,2A**).

315 ***NSCs Provide an Efficient Therapeutic Cargo Delivery System:*** Our results demonstrate that the
316 impressive tumor tropism of NSCs to IP metastases may significantly advance peritoneal chemotherapy by
317 guiding the delivery of pre-loaded therapeutic cargo. We observed that, whereas the localization of NPs to
318 tumors is low when they are delivered freely (perhaps because they are engulfed by peritoneal or tumor-
319 associated macrophages), their tumor localization was significantly (more than 60%) greater when they were
320 delivered within NSCs. We believe that this improvement can be generalized to other free vs. NSC-delivered
321 therapeutic payloads. For example, we have previously reported improved NSC-mediated drug delivery of two
322 standard-of-care chemotherapeutic drugs, cisplatin [13] and paclitaxel (PTX)[14] to peritoneal metastases.

323 One critical insight yielded by the current study was that the NSCs localized primarily to the peritumoral
324 stroma, with limited penetration into the tumor parenchyma. Thus, it is possible that improving the delivery of a
325 drug to tumor nodules using NSCs may not be sufficient to improve its efficacy if other parameters dominate
326 the response to treatment. For example, NSC-mediated drug delivery only improved the therapeutic efficacy of

PTX [14] but not cisplatin (unpublished data). Other important parameters include: diffusion limits [cisplatin (200 cell layers) vs PTX (80 layers)[28]]; peritoneal-to-plasma area under the concentration-time curve ratio [cisplatin (7.8-21) [29, 30] vs PTX (853) [31]]; treatment schedule [cisplatin (slow release, treated weekly) vs PTX (burst release, treated bi-weekly); impaired biological activity of cisplatin after release from NSCs, microenvironmental priming by PTX that improves drug penetration or immune stimulation upon repeated dose cycles [32-36]. It will be important to consider and address these factors when selecting and developing therapeutic cargo for effective NSC delivery.

NSC Safety Considerations: Our results also indicate that HB1.F3.CD21 NSCs do not engraft, and are not viable long-term within the peritoneal tumor setting, dying off within approximately two weeks. Furthermore, they are non-tumorigenic in the peritoneal setting, consistent with our current clinical data in the glioma setting, as patients in phase I trials of allogeneic NSC-mediated enzyme/prodrug and CRAd-S-pk7 treatments have tolerated multiple intracranial administrations without adverse events or evidence of secondary tumorigenicity [15]. In stark contrast, MSCs have been reported to functionally engraft into peritoneal organs [37, 38], and can promote ovarian tumor growth by inducing the expression of IL-1, associating with macrophages, and transforming into carcinoma-associated MSCs [39]. IP MSC administration has also been shown to increase pro-inflammatory cytokines in mice, triggering such dramatic omental immune cell influx that the organ doubled in weight [40]. The results presented here show that NSCs induce negligible immunological recognition *in vitro*; however, further investigation of the potential immunomodulatory effects of NSCs within the IP cavity will be important within the context of future therapeutic efficacy studies, particularly for repeated NSC administrations.

CONCLUSION

This allogeneic, immortalized, GMP-grade NSC line has significant practical and economic advantages over autologous cell-carriers. It provides a non-tumorigenic, “off-the-shelf” platform that is readily available for

modification, scale-up, and banking. Furthermore, it is amenable to the delivery of a broad array of therapeutic payloads within the peritoneal cavity. Our translational interest is in developing these cells for improved delivery of drug-loaded NPs, oncolytic viruses, and other promising therapeutic cargo, including bispecific T-cell engagers, small interfering RNA, and antibodies to patients with abdominal metastatic disease. Our long-term vision is to introduce cargo-loaded NSCs after surgical debulking. Surgical trauma creates disruptions to the patient's mesothelial layer which serve as privileged sites for cancer cell attachment [41, 42]. However, we anticipate that NSCs will also be attracted to these regions and may be able to deliver a therapeutic dose strong enough to eliminate the attached tumor cells, thus preventing new tumor development.

LIST OF ABBREVIATIONS:

AuNR: gold nanorod; **NSC:** neural stem cell; **MSC:** mesenchymal stem cell; **RNA:** Ribonucleic acid; **DNA:** Deoxyribonucleic acid; **NP:** nanoparticle; **GMP:** good manufacturing practice; **IL-1:** Interleukin 1; **PTX:** paclitaxel; **PCR:** polymerase chain reaction; **FACS:** fluorescence-activated cell sorting; **IP:** Intraperitoneal; eGFP: green fluorescent protein; **ffluc:** firefly luciferase; **ICP-MS:** inductively coupled plasma mass spectrometry; **MHC:** major histocompatibility complex; **PBMC:** peripheral blood mononuclear cells; **HLA**: human leukocyte antigen

DECLARATIONS

Ethics approval and consent to participate: N/A

Consent for publication: N/A

Availability of data and materials: All data generated or analyzed during this study are included in this published article [and its supplementary information files].

Competing Interests: K.S.A., J.B., and R.M. disclose intellectual property with City of Hope and Harvard Patents. All other authors declare no competing interests.

Funding: This work was supported by the Rosalinde and Arthur Gilbert Foundation, City of Hope Women's Cancer Program, the California Institute of Regenerative Medicine Training Program (grant EDUC2-08383, TRAN1-11544), the Alvarez Family Foundation, the Anthony F. and Susan M. Markel Foundation, the Daphna and Richard Ziman Family Foundation, the National Cancer Institute (grant 1R01CA197359), the H.N. and Frances C. Berger Foundation, and the Norman and Melinda Payson Fellowship. Inductively coupled mass spectrometry and mixed lymphocyte reactions were performed by the City of Hope Analytical Pharmacology Core, which is supported by the National Cancer Institute of the National Institutes of Health under award number P30CA033572.

Authors' contributions: Jennifer Batalla-Covello: Design, Collection of data, Manuscript writing; Wafa Abidi: Collection and analysis of data; Hoi Wa Ngai: Assembly of data; Caitlyn Hyde: Collection of data; Diana Machado: Collection of data; Asma Abdul-Majid: Collection of data; Mohamed Hammad: Design, Collection of data; Linda Flores: Design, Collection of data; Greg Copeland: Design; Thanh Dellinger: Financial Support, Final Approval of Manuscript; Ernest Han: Final Approval; Jacob Berlin: Conception, Design, Financial Support, Interpretation of data, Final Approval; Karen S. Aboody: Conception, Design, Data Review, Financial Support, Final Approval; Rachael Mooney: Conception, Design, Collection/Assembly/Analysis/Interpretation of data, Writing

Acknowledgements: We thank scientific editor Kerin K. Higa, Ph.D.

REFERENCES

1. Lengyel, E., *Ovarian cancer development and metastasis.* Am J Pathol, 2010. **177**(3): p. 1053-64.
2. Huang, B., et al., *Active targeting of chemotherapy to disseminated tumors using nanoparticle-carrying T cells.* Sci Transl Med, 2015. **7**(291): p. 291ra94.
3. Stephan, M.T., et al., *Therapeutic cell engineering with surface-conjugated synthetic nanoparticles.* Nat Med, 2010. **16**(9): p. 1035-41.
4. Choi, M.-R., et al., *A Cellular Trojan Horse for Delivery of Therapeutic Nanoparticles into Tumors.* Nano Letters, 2007. **7**(12): p. 3759-3765.
5. Li, L., et al., *Silica Nanorattle–Doxorubicin-Anchored Mesenchymal Stem Cells for Tumor-Tropic Therapy.* ACS Nano, 2011. **5**(9): p. 7462-7470.
6. Mooney, R., et al., *Conjugation of pH-responsive nanoparticles to neural stem cells improves intratumoral therapy.* J Control Release, 2014. **191**: p. 82-9.
7. Kendall, S.E., et al., *Neural stem cell targeting of glioma is dependent on phosphoinositide 3-kinase signaling.* Stem Cells, 2008. **26**(6): p. 1575-86.
8. Mirahmadi, N., et al., *Effect of liposome size on peritoneal retention and organ distribution after intraperitoneal injection in mice.* International Journal of Pharmaceutics, 2010. **383**(1): p. 7-13.
9. Lu, Z., et al., *Tumor-penetrating microparticles for intraperitoneal therapy of ovarian cancer.* The Journal of pharmacology and experimental therapeutics, 2008. **327**(3): p. 673-682.
10. De Smet, L., et al., *Optimization of drug delivery systems for intraperitoneal therapy to extend the residence time of the chemotherapeutic agent.* ScientificWorldJournal, 2013. **2013**: p. 720858.
11. Mader, E.K., et al., *Mesenchymal stem cell carriers protect oncolytic measles viruses from antibody neutralization in an orthotopic ovarian cancer therapy model.* Clin Cancer Res, 2009. **15**(23): p. 7246-55.
12. Mader, E.K., et al., *Optimizing patient derived mesenchymal stem cells as virus carriers for a phase I clinical trial in ovarian cancer.* J Transl Med, 2013. **11**: p. 20.
13. Cao, P., et al., *Intraperitoneal Administration of Neural Stem Cell–Nanoparticle Conjugates Targets Chemotherapy to Ovarian Tumors.* Bioconjugate Chemistry, 2017. **28**(6): p. 1767-1776.
14. Tiet, P., et al., *Silica Coated Paclitaxel Nanocrystals Enable Neural Stem Cell Loading For Treatment of Ovarian Cancer.* Bioconjug Chem, 2019. **30**(5): p. 1415-1424.
15. Portnow, J., et al., *Neural Stem Cell-Based Anticancer Gene Therapy: A First-in-Human Study in Recurrent High-Grade Glioma Patients.* Clin Cancer Res, 2017. **23**(12): p. 2951-2960.
16. Tirughana, R., et al., *GMP Production and Scale-Up of Adherent Neural Stem Cells with a Quantum Cell Expansion System.* Mol Ther Methods Clin Dev, 2018. **10**: p. 48-56.
17. Mooney, R., et al., *Enhanced Delivery of Oncolytic Adenovirus by Neural Stem Cells for Treatment of Metastatic Ovarian Cancer.* Mol Ther Oncolytics, 2019. **12**: p. 79-92.
18. Cheng, Y., et al., *Nanoparticle-Programmed Self-Destructive Neural Stem Cells for Glioblastoma Targeting and Therapy.* Small, 2013. **9**(24): p. 4123-4129.
19. Ray, A. and B.N. Dittel, *Isolation of mouse peritoneal cavity cells.* Journal of visualized experiments : JoVE, 2010(35): p. 1488.
20. Fiala, J.C., *Reconstruct: a free editor for serial section microscopy.* J Microsc, 2005. **218**(Pt 1): p. 52-61.
21. Metz, M.Z., et al., *Neural stem cell-mediated delivery of irinotecan-activating carboxylesterases to glioma: implications for clinical use.* Stem Cells Transl Med, 2013. **2**(12): p. 983-92.
22. Mooney, R., et al., *Neural Stem Cell-Mediated Intratumoral Delivery of Gold Nanorods Improves Photothermal Therapy.* ACS Nano, 2014. **8**(12): p. 12450-12460.
23. Schnarr, K., et al., *Gold Nanoparticle-Loaded Neural Stem Cells for Photothermal Ablation of Cancer.* Advanced Healthcare Materials, 2013. **2**(7): p. 976-982.
24. Sodek, K.L., et al., *Cell-cell and cell-matrix dynamics in intraperitoneal cancer metastasis.* Cancer metastasis reviews, 2012. **31**(1-2): p. 397-414.
25. Ahmed, A.U., et al., *A Preclinical Evaluation of Neural Stem Cell–Based Cell Carrier for Targeted Antiglioma Oncolytic Virotherapy.* JNCI: Journal of the National Cancer Institute, 2013. **105**(13): p. 968-977.

26. Ziu, M., et al., *Glioma-produced extracellular matrix influences brain tumor tropism of human neural stem cells.* J Neurooncol, 2006. **79**(2): p. 125-33.
27. Lassailly, F., E. Griessinger, and D. Bonnet, *"Microenvironmental contaminations" induced by fluorescent lipophilic dyes used for noninvasive in vitro and in vivo cell tracking.* Blood, 2010. **115**(26): p. 5347-5354.
28. Los, G., et al., *Platinum distribution in intraperitoneal tumors after intraperitoneal cisplatin treatment.* Cancer Chemother Pharmacol, 1990. **25**(6): p. 389-94.
29. Carlier, C., et al., *Tumour tissue transport after intraperitoneal anticancer drug delivery.* International Journal of Hyperthermia, 2017. **33**(5): p. 534-542.
30. Heldin, C.H., et al., *High interstitial fluid pressure - an obstacle in cancer therapy.* Nat Rev Cancer, 2004. **4**(10): p. 806-13.
31. Levine, E.A. and W.P. Ceelen, *Intraperitoneal Cancer Therapy : Principles and Practice*. 2015, Boca Raton: CRC Press.
32. Kampan, N.C., et al., *Paclitaxel and Its Evolving Role in the Management of Ovarian Cancer.* Biomed Res Int, 2015. **2015**: p. 413076.
33. Kuh, H.J., et al., *Determinants of paclitaxel penetration and accumulation in human solid tumor.* J Pharmacol Exp Ther, 1999. **290**(2): p. 871-80.
34. Jang, S.H., M.G. Wientjes, and J.L. Au, *Enhancement of paclitaxel delivery to solid tumors by apoptosis-inducing pretreatment: effect of treatment schedule.* J Pharmacol Exp Ther, 2001. **296**(3): p. 1035-42.
35. Lu, D., et al., *Tumor priming enhances delivery and efficacy of nanomedicines.* J Pharmacol Exp Ther, 2007. **322**(1): p. 80-8.
36. Jang, S.H., M.G. Wientjes, and J.L. Au, *Determinants of paclitaxel uptake, accumulation and retention in solid tumors.* Invest New Drugs, 2001. **19**(2): p. 113-23.
37. Wilson, T., et al., *Fate of bone marrow-derived stromal cells after intraperitoneal infusion or implantation into femoral bone defects in the host animal.* J Tissue Eng, 2010. **2010**: p. 345806.
38. Meyerrose, T.E., et al., *In vivo distribution of human adipose-derived mesenchymal stem cells in novel xenotransplantation models.* Stem Cells, 2007. **25**(1): p. 220-7.
39. Gao, T., et al., *Human mesenchymal stem cells in the tumour microenvironment promote ovarian cancer progression: the role of platelet-activating factor.* BMC Cancer, 2018. **18**(1): p. 999.
40. Bazhanov, N., et al., *Intraperitoneally infused human mesenchymal stem cells form aggregates with mouse immune cells and attach to peritoneal organs.* Stem cell research & therapy, 2016. **7**: p. 27-27.
41. Bergstrom, M., M.L. Ivarsson, and L. Holmdahl, *Peritoneal response to pneumoperitoneum and laparoscopic surgery.* Br J Surg, 2002. **89**(11): p. 1465-9.
42. Oosterling, S.J., et al., *Surgical trauma and peritoneal recurrence of colorectal carcinoma.* Eur J Surg Oncol, 2005. **31**(1): p. 29-37.

SUPPPLEMENTARY INFORMATION

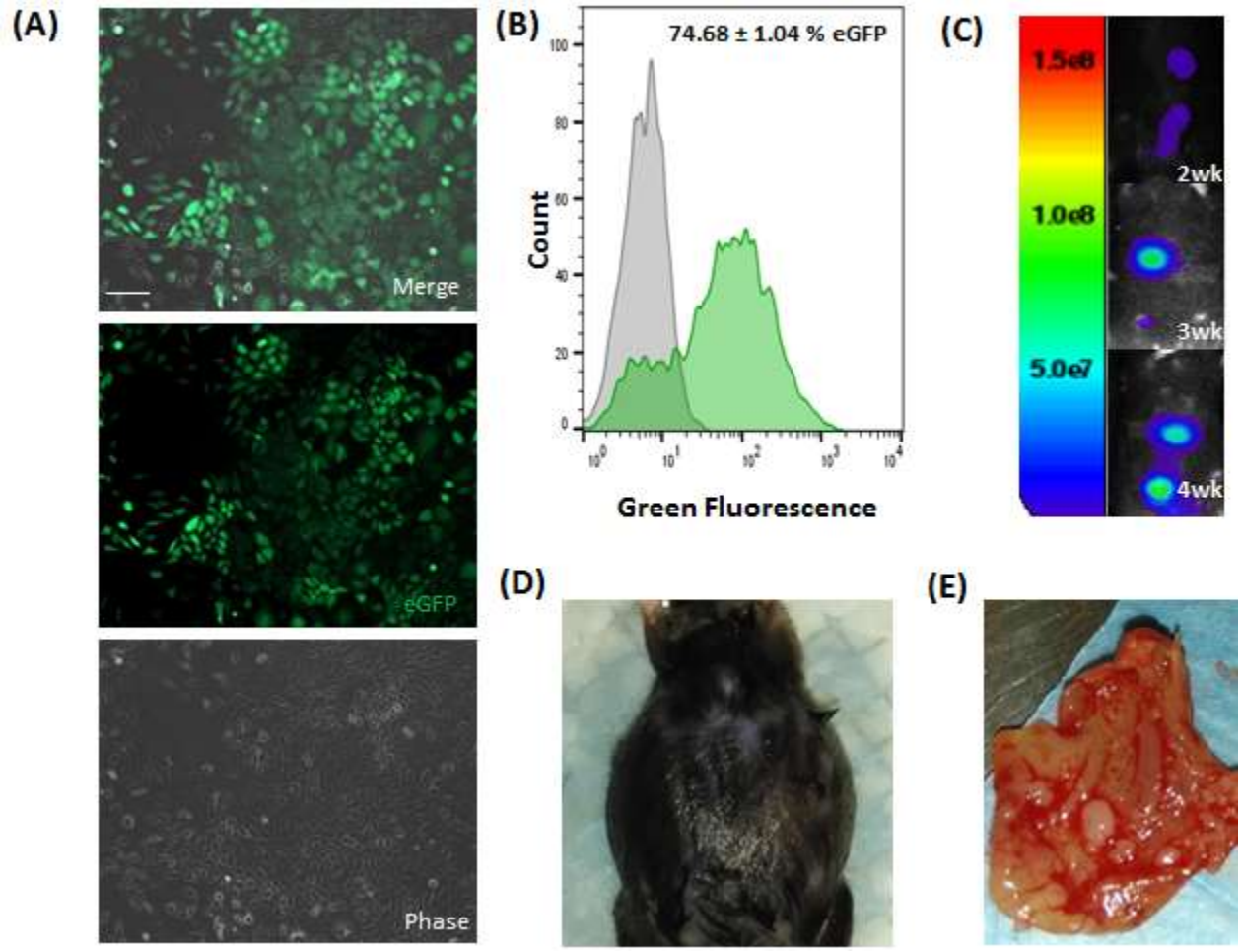

Supplementary Figure 1. Murine ID8 ovarian cancer cell line modified to stably express green fluorescent protein (eGFP) and firefly luciferase (ffluc). (A): Phase and fluorescence microscopy images of eGFP-positive ID8 (ID8.eGFP.ffluc) cells five days post-infection. Scale bar = 50 µm. **(B):** Representative histogram of ID8.eGFP.ffluc cells quantified by flow cytometry 15 days after infection. **(C):** Bioluminescent images confirming tumor engraftment after peritoneal administration of 5×10^6 ID8.eGFP.ffluc cells into immunocompetent C57Bl/6 mice, color scale bar shown in relative light units. **(D):** Representative photograph demonstrating the development of ascites in a C57Bl/6 mouse, two months after inoculation with ID8.eGFP.ffluc cells. **(E):** *Ex vivo* photograph of the peritoneal wall harvested from a C57Bl/6 mouse inoculated with ID8.eGFP.ffluc cells.